Manuscript Details

Manuscript number	JAG_2018_417_R1
Title	Full year crop monitoring and separability assessment with fully-polarimetric L-band UAVSAR: a case study in the Sacramento Valley, California
Article type	Research Paper

Abstract

Spatial and temporal information on plant and soil conditions is needed urgently for monitoring of crop productivity. Remote sensing has been considered as an effective means for crop growth monitoring due to its timely updating and complete coverage. In this paper, we explored the potential of L-band fully-polarimetric Uninhabited Aerial Vehicle Synthetic Aperture Radar (UAVSAR) data for crop monitoring and classification. The study site was located in the Sacramento Valley, in California where the cropping system is relatively diverse. Full season polarimetric signatures, as well as scattering mechanisms, for several crops, including almond, walnut, alfalfa, winter wheat, corn, sunflower, and tomato, were analyzed with linear polarizations (HH, HV, and VV) and polarimetric decomposition (Cloude–Pottier and Freeman–Durden) parameters, respectively. The separability amongst crop types was assessed across a full calendar year based on both linear polarizations and decomposition parameters. The unique structure-related polarimetric signature of each crop was provided by multitemporal UAVSAR data with a fine temporal resolution. Permanent tree crops (almond and walnut) and alfalfa demonstrated stable radar backscattering values across the growing season, whereas winter wheat and summer crops (corn, sunflower, and tomato) presented drastically different patterns, with rapid increase from the emergence stage to the peak biomass stage, followed by a significant decrease during the senescence stage. In general, the polarimetric signature was heterogeneous during June and October, while homogeneous during March-to-May and July-to-August. The scattering mechanisms depend heavily upon crop type and phenological stage. The primary scattering mechanism for tree crops was volume scattering (>40%), while surface scattering (>40%) dominated for alfalfa and winter wheat, although double-bounce scattering (>30%) was notable for alfalfa during March-to-September. Surface scattering was also dominant (>40%) for summer crops across the growing season except for sunflower and tomato during June and corn during July-to-October when volume scattering (>40%) was the primary scattering mechanism. Crops were better discriminated with decomposition parameters than with linear polarizations, and the greatest separability occurred during the peak biomass stage (July-August). All crop types were completely separable from the others when simultaneously using UAVSAR data spanning the whole growing season. The results demonstrate the feasibility of L-band SAR for crop monitoring and classification, without the need for optical data, and should serve as a guideline for future research.

Keywords	Multi-temporal image; full-polarimetric SAR; crop growth monitoring; polarimetric decomposition; scattering mechanisms; classification.
Taxonomy	Classification, Mapping, Multi-Temporal Image

Corresponding Author	Huapeng Li
Order of Authors	Huapeng Li, Ce Zhang, Shuqing Zhang, Pete Atkinson

Suggested reviewers	Steven de Jong, Qunming Wang, Victor Rodriguez-Galiano, Tiejun Wang, Jadu Dash

Submission Files Included in this PDF

File Name [File Type]

JAG Cover letter.pdf [Cover Letter]

JAG revision Response letter.pdf [Response to Reviewers]

JAG Highlights.pdf [Highlights]

JAG revision Manuscript.pdf [Manuscript File]

JAG revision Figures.pdf [Figure]

JAG revision Tables.pdf [Table]

Dear Dr. Abel Ramoelo, Associate Editor,

Prof. van der Meer, Editor-in-Chief,

International Journal of Applied Earth Observations and Geoinformation

On behalf of my co-authors, we thank you very much for giving us the opportunity to revise the manuscript, and we are grateful to two reviewers for their constructive comments and suggestions on our manuscript titled "Full year crop monitoring and separability assessment with fully-polarimetric L-band UAVSAR: a case study in the San Joaquin Valley, California" (Former Ref: JAG_2018_417).

We have revised the manuscript carefully according to the comments, and highlighted the revisions in the revised manuscript using the blue text. In our point-by-point response letter attached below, the comments of each reviewer are provided in plain text followed by our responses in blue text. The major revisions we have made include:

1. Unnecessary detail about the previous works were removed to make the structure of the introduction section clear.
2. The bullet point summary of the research was rephrased to match the contents of the results and discussion sections.
3. The results section was carefully revised according to the comments to make the analysis clear.
4. Some important literature recommended by the reviewers were included in the paper.
5. Crop classification results using two machine learning algorithms with different UAVSAR features (linear polarizations and polarimetric parameters) were included in the results section.

We trust that you will find the revised manuscript acceptable for publication in *International Journal of Applied Earth Observations and Geoinformation*.

Looking forward to hearing from you.

Best wishes

Professor Peter M. Atkinson

Dean, Faculty of Science and Technology,

Lancaster University,

Tel: 01524 595203

Email: pma@lancaster.ac.uk

Response to Reviewers

We are grateful to the anonymous reviewers for their constructive comments and suggestions, and have carefully revised the manuscript in response to their advice. The comments of each reviewer in plain text followed by our responses in blue text are provided below.

Referee: 1

Comments to the Author

Main comments

(1) This paper uses fully polarimetric L-band UAVSAR data to analyze the polarimetric signature and scattering mechanisms of a mixture of perennial and annual crops in California over the course of a full calendar year. While the paper is plainly inspired by Whelen and Siqueira (2017), it is clear that the authors have taken this subject further, extending the analysis to cover a more complexly cropped region, and using the polarimetric signatures to characterize scattering behavior and crop separability. The authors also made logical connections between the scattering behavior and crop phenology during specific times of the year, showing how this explained some of the separability results.

Response (R): Thank you very much for reviewing our manuscript and making a brief summary for our work.

(2) While the research appears to be adequate, the text could use improvements. As this is not a review article, the introduction goes into unnecessary detail about some of the citations. The bullet point summary of research at the end of the introduction is confusing, and needs rephrasing to match what is covered in the results and discussion sections. The results section could also be revised to improve the clarity of the analysis. While overall the authors do a good job of connecting their work with previous research, numerous improvements could be made to the cited literature.

Response (R): Many thanks for providing us with these very careful and constructive comments. We have revised the manuscript carefully according to the comments and responded to them point by point as below.

Specific comments

(1) The study site is located in the Sacramento Valley, not the San Joaquin Valley. Please adjust title and text accordingly.

R: Thank you for this comment. We have revised the title and text as suggested.

> "Full year crop monitoring and separability assessment with fully-polarimetric L-band UAVSAR: a case study in the Sacramento Valley, California" **(page 1, line 2-3).**

(2) Almonds and walnuts are not normally referred to as fruits in English – please refer to them as nut trees, nut crops, tree crops, or orchards, but not as fruit trees.

R: Thank you for this comment. We have replaced 'fruit trees' with 'tree crops' throughout the text as suggested.

(3) Generally it is not desired to cite unpublished papers, especially if they are by other authors. Canisius et al., now has an issue number and date assigned to it – please update.

R: Thank you for this suggestion. We updated the reference by Canisius et al. (2018).

(4) Introduction paragraph 2 – second sentence unnecessary.

R: Agreed. We deleted the sentence as suggested.

(5) Introduction paragraph 3 – Suri et al., 2010 is about urban areas, not agricultural land.

R: Thank you for this careful comment. We removed the reference.

(6) Introduction paragraph 3 – unnecessary to list all the previous satellites – the second half of this paragraph could be more concise.

R: Thank you for this suggestion. We have shortened the second half of the paragraph as follows:

"The main SAR data sources employed by previous crop research involve satellite RADARSAT-1/2 (Choudhury et al., 2006), ENVISAT ASAR (Bouvet et al., 2009), and ALOS PALSAR (McNairn et al., 2009b). However, the majority of these data were restricted to single polarization (e.g. RADARSAT-1) or dual-polarization modes (e.g. ASAR), which greatly limits the practical utility of SAR for crop classification." **(page 4, line 81-86)**.

(7) Introduction paragraphs 5 and 6 – unnecessary detail given about specific past works; this isn't a review article.

R: Agreed. We have deleted the details about previous works as suggested.

"The seasonal patterns of these scattering mechanisms rely heavily on crop type and phenological stages, in which unique information for crop monitoring and identification is potentially provided (e.g. McNairn et al., 2009b; Adams et al., 2013; Jiao et al., 2014; Canisius et al., 2018). " **(page 5, line 98-101)**.

"However, there have been very few studies of crop characterization using full-polarimetric L-band SAR (McNairn et al., 2009b; Skriver, 2012; Whelen and Siqueira, 2017) " **(page 5, line 113-115)**.

(8) Introduction paragraph 6 – additional fully polarimetric L-band agricultural studies include AgriSAR campaigns in Germany, and AIRSAR projects.

R: Thank you for this comment. We have added the related contents in the paragraph and rewritten the sentence as follows:

"However, there have been very few studies of crop characterization using full-polarimetric L-band SAR (McNairn et al., 2009b; Skriver, 2012; Whelen and Siqueira, 2017), even though some research projects were conducted to collect such data, such as the AgriSAR campaign in Germany (Skriver, 2011) and the Multisensor Airborne Campaign in Italy and Sweden (Macelloni et al., 2001)." **(page 5, line 113-118)**.

(9) Introduction paragraph 7 – the three bullet points overlap with each, contain multiple items in one bullet point, and do not match how the analysis is organized in the results and discussion.

R: Yes, we fully agree with this valuable comment. We have rephrased the bullet points to match the analysis in the results and discussion sections:

> " (1) L-band fully-polarimetric UAVSAR was used for the first time to characterize the seasonal patterns in radar response for tree crops (almond, walnut) as well as other crop types (alfalfa, winter wheat, corn, sunflower, and tomato).
>
> (2) The contributions of scattering mechanisms to radar response were quantified for different crop types, and the seasonal variation in three different scattering mechanisms was analysed.
>
> (3) The separability amongst crop types was assessed and analyzed through the growing season using full calendar year time-series UAVSAR, and this serves as an important guide for future UAVSAR-based crop classification." **(page 6, line 127-135)**.

(10) Section 3.1 paragraph 1 – UAVSAR is flown off a Gulfstream platform.

R: Thank you for this comment. We have rewritten this sentence as follows:

> "The radar is mounted onboard a Gulfstream-3 aircraft flown at an altitude of 12.5 km (Chapman et al., 2011)" **(page 7-8, line 167-168)**.

(11) Section 3.1 paragraph 2 – Chapman et al., 2011 would be a more appropriate paper to cite for UAVSAR technical specifications.

R: Agreed. We have included this literature into the paper.

> "No further speckle filters were applied since the multiplicative noise (speckle) contained in the SAR images was reduced significantly by the multilook processing (Chapman et al., 2011) " **(page 8, line 182-184)**.

(12) Section 3.3 paragraph 2 – Was the technique of inwardly buffering fields by one pixel gotten from Whelen and Siqueira (2017)? If so, please cite.

R: Thank you for this question. We have cited the reference in the text.

> "Second, each identified crop field was outlined manually and buffered inwardly from the field boundary by one pixel (Whelen and Siqueira, 2017) " **(page 11, line 244-245)**.

(13) Section 4.1 paragraph 2 – cite specific, original documents – i.e. which California Ag Statistics document on that website, the CDL doesn't include a crop calendar, and Whelen and Siqueira's (2017) crop calendar is cited directly from a USDA source.

R: Thank you for this valuable suggestion. We have shortened the sentence and added the website that directly provides the original data source of the crop calendar used in our paper.

> "Drawing on official statistics (California Agricultural Statistics, 2011; USDA-NASA, 2011 (a)), calendars of the studied crops are summarized in Fig. 4." **(page 13, line 296-297)**.

> "USDA NASS, 2011 (a). Crop Progress. Retrieved January 13, 2018, from. http://usda.mannlib.cornell.edu/MannUsda/viewDocumentInfo.do;jsessionid=A8F0A37CA76B0F6E77E0FDE1E10BA5F9?documentID=1048/." **(page 28, line 711-713)**.

(14) Section 4.1 paragraph 3 – confusing organization of this paragraph.

R: Many thanks for this comment. We have reorganized this paragraph to make the presentation clear and logical:

> " It should be noted that the calendar for the same crop may vary between different areas due to natural conditions (e.g. weather conditions, soil water content, and field slope) and farmer decisions (Saich and Borgeaud, 2000). To demonstrate such variation clearly, the standard deviation (STD) profile of the HV polarization signatures for each crop are shown in Fig. 3(d). Seasonal patterns of STD for the permanent crops (i.e. almond, walnut, and alfalfa) are comparable and relatively

stable (about 2~4 dB), with a general downward trend over the growing season. Winter wheat had small STD values (below 3 dB) during January-to-May, but relatively large values (over 3.5 dB) during June-to-October, which might be attributable to the second planting of some harvested fields. As for the summer crops, two STD peaks (generally > 5 dB) were conspicuous in the profiles. The first occurred during June, caused by the difference in growth time amongst crops, while the second occurred during October, caused by the difference in harvesting time (Figs. 3(d) and 4). To highlight such field-to-field spatial variation, the HV polarization during the growing season (March to October) is shown in Fig. 5, in which typical fields for each crop are marked by black patches. In general, the results were consistent with the analysis of the STD in the HV polarization. That is, the radar signature of crops was heterogeneous in the June and October images, but homogeneous in the images dated March, May, July and August." **(page 14-15, line 321-338)**.

(15) Section 4.3 paragraph 1 – the JM patterns and greater separability of polarimetric decompositions over linear polarizations are not clear in Figure 8.

R: Agreed. We redrew the figure in which grid lines were added to present the comparison of crop separability between polarimetric parameters and linear polarizations clearly. Please refer to the revision.

(16) Section 4.3 paragraph 2 – which images (or months) are defined as the growing season?

R: Thank you for this question. We defined the growing season in the paragraph:

> "The separability was found to vary over the growing season (March to October) due to the specific calendars and structures of crops." **(page 18, line 414-415)**.

(17) Section 5 paragraph 4 – why do describe sunflower and tomatoes as having a dense structure as compared to corn?

R: Thank you for this question. We explained the reason in the text and added a new figure (Fig. 9) to illustrate this. Please refer to the revision.

"In comparison with the dense structure (crowded and horizontally oriented leaves) of sunflower and tomato, corn has sparse and randomly oriented leaves (Fig. 9), which exert less impact on the penetration of the radar signal, even during the peak biomass stage. " **(page 21-22, line 508-511)**.

"Fig. 9. Summer crop examples for corn, sunflower, and tomato. Note that all the photos were taken in the United States by volunteers, and are freely shared by the Earth Observation and Modeling Facility (EOMF) at the University of Oklahoma (http://eomf.ou.edu/visualization/gmap/).".

(18) Section 6 paragraph 4 – McNairn et al., 2009a used C-band, and took HH and VV/VH from two different SAR systems. This comparison is like comparing apples and oranges, and does not support your point well.

R: Many thanks for this comment. We have removed this sentence.

(19) References - Silva et al., 2009 is listed in references but not in the text.

R: Many thanks for this careful comment. We have included the reference in the text.

"Synthetic aperture radar (SAR) is receiving increasing attention since SAR instruments can acquire data regardless of the weather conditions and cloud cover by operating at wavelengths that can penetrate clouds (Silva et al., 2009; Skriver, 2012)" **(page 4, line 73-75)**.

(20) Figure 1 caption – “agricultural region” instead of “agricultural district”

R: Agreed. We have revised the caption as suggested.

"Fig. 1. The study site in the agricultural region of the Sacramento Valley California.".

(21) Figure 2 – If you manually traced fields, then why are multiple visually distinct fields in Fig 2a merged into one polygon in Figure 2b?

R: Many thanks for this comment. This is because these fields were identified as one polygon in the CDL map. By further checking these fields in the UAVSAR image, we found that the boundaries amongst them were not very clear. We, therefore, merged them into one polygon in the manual interpretation procedure.

(22) Figure 2a – Please specify which bands are R, G, and B.

R: Thank you for this comment. We revised the caption as follows:

> "Fig. 2. (a) The UAVSAR image dated 20 July, 2011 (R-G-B, bands VV, HV, and HH), (b) the outlined crop fields.".

(23) Figure 5 – needs a legend and a scale

R: Thank you for this comment. We rectified the figure as suggested. Please refer to the revision.

(24) Table 1 – remove the two columns with identical values for all entries, and instead put in the caption or text that all images were in PolSAR mode and there was no snow.

R: Thank you for this valuable suggestion. We revised the Table as suggested. Please refer to the revision.

> "Table 1. Detailed description of UAVSAR data acquisitions in 2011 and the corresponding weather conditions; meteorological data were acquired from a station (in the city of Sacramento) located next to the study area. All images were in PolSAR (polarimetric SAR) mode and there was no snow.".

Referee: 2

Comments to the Author

1. This paper proposed to use L-band UAVSAR for better separation of crops for reliable crop monitoring. Generally, the paper is well-organized and well-written, with a plenty of nice figures (results) for illustration. I only have some minor comments.

R: Many thanks for reviewing our paper and providing us with valuable suggestions.

2. The main motivation of the study is for more separable recognition of crops in classification. The authors only analyzed the rational of the method, but not conducted any experimental validation for the point of "better classification performance". I have only found the calculation of JM distance. This is not sufficient for quantitative assessment. In my opinion, any standard classification method should be performed and the performance of "not using L-band" and "using L-band" needs to be compared. This is a critical part for validation of your idea proposed in the paper.

R: Many thanks for this constructive comment. We fully agree that only JM distance result was not sufficient to support our claim that polarimetric parameters perform better than linear polarizations in crop discrimination. To further validate this, we compared the classification accuracies achieved by the MLP and SVM classifiers, respectively, using different features of UAVSAR (linear polarizations, polarimetric parameters, and all features). The classification accuracy was generally in accordance with the analysis of JM-distance, which demonstrates the unique value of polarimetric parameters in crop classification. We have thoroughly included the classification results in the text as follows:

> "To further validate the potential of UAVSAR in crop discrimination, two machine learning algorithms, the Multi-layer Perceptron (MLP) and Support Vector Machine (SVM), were employed using different features (linear polarizations and polarimetric parameters). The control parameters of the MLP were set by following the recommendations of Zhang et al. (2018). The most suitable radial basis function (RBF) kernel SVM was used in this research, with the parameters being optimized through a grid search method with five-fold cross validation (Barrett et al., 2014). Table 3 summarizes the classification accuracy assessment, including the overall accuracy (OA) and Kappa coefficient (*k*). The OA and *k* produced by different features using both algorithms were in accordance with the

analysis of JM distance. As shown in Table 3, the CP and FD decomposition parameters produced consistently greater accuracy in comparison to the linear polarizations, with OA = 93.01% and 93.71% by MLP, and OA = 92.03% and 93.01% by SVM, respectively; the combined use of all features (linear polarizations and polarimetric parameters) achieved the largest classification OA, with up to 95.80% using MLP and 97.48% using SVM, respectively. Such coherency of classification accuracy further supports the analysis of JM distance, and demonstrates the unique value of polarimetric parameters in SAR-based crop classification. " **(page 18-19, line 437-453)**.

" Table 3. Classification accuracy achieved by the MLP and SVM algorithms with linear polarizations (LP), CP decomposition parameters (CP), FD decomposition parameters (FD), and all features (All). Note that OA denotes overall accuracy, and *k* is the Kappa coefficient.".

Highlight

1. L-band fully-polarimetric UAVSAR was used for the first time to characterize the seasonal patterns in radar response for tree crops (almond, walnut) as well as other crop types (alfalfa, winter wheat, corn, sunflower, and tomato).
2. The contributions of scattering mechanisms to radar response were quantified for different crop types, and the seasonal variation in three different scattering mechanisms was analysed.
3. The separability amongst crop types was assessed and analyzed through the growing season using full calendar year time-series UAVSAR.

Full year crop monitoring and separability assessment with fully-polarimetric L-band UAVSAR: a case study in the Sacramento Valley, California

Huapeng Li [a, b*], Ce Zhang [b], Shuqing Zhang [a], Peter M. Atkinson [b,*]

[a] Northeast Institute of Geography and Agroecology, Chinese Academy of Sciences, Changchun 130012, China

[b] Lancaster Environment Centre, Lancaster University, Lancaster LA1 4YQ, UK

Abstract

Spatial and temporal information on plant and soil conditions is needed urgently for monitoring of crop productivity. Remote sensing has been considered as an effective means for crop growth monitoring due to its timely updating and complete coverage. In this paper, we explored the potential of L-band fully-polarimetric Uninhabited Aerial Vehicle Synthetic Aperture Radar (UAVSAR) data for crop monitoring and classification. The study site was located in the Sacramento Valley, in California where the cropping system is relatively diverse. Full season polarimetric signatures, as well as scattering mechanisms, for several crops, including almond, walnut, alfalfa, winter wheat, corn, sunflower, and tomato, were analyzed with linear polarizations (HH, HV, and VV) and polarimetric decomposition (Cloude–Pottier and Freeman–Durden) parameters, respectively. The separability amongst crop types was assessed across a full calendar year based on both linear polarizations and decomposition parameters. The unique structure-

[*] Corresponding author.
E-mail addresses: lihuapeng@neigae.ac.cn (H.P. Li), pma@lancaster.ac.uk (P.M. Atkinson).

related polarimetric signature of each crop was provided by multitemporal UAVSAR data with a fine temporal resolution. Permanent tree crops (almond and walnut) and alfalfa demonstrated stable radar backscattering values across the growing season, whereas winter wheat and summer crops (corn, sunflower, and tomato) presented drastically different patterns, with rapid increase from the emergence stage to the peak biomass stage, followed by a significant decrease during the senescence stage. In general, the polarimetric signature was heterogeneous during June and October, while homogeneous during March-to-May and July-to-August. The scattering mechanisms depend heavily upon crop type and phenological stage. The primary scattering mechanism for tree crops was volume scattering (>40%), while surface scattering (>40%) dominated for alfalfa and winter wheat, although double-bounce scattering (>30%) was notable for alfalfa during March-to-September. Surface scattering was also dominant (>40%) for summer crops across the growing season except for sunflower and tomato during June and corn during July-to-October when volume scattering (>40%) was the primary scattering mechanism. Crops were better discriminated with decomposition parameters than with linear polarizations, and the greatest separability occurred during the peak biomass stage (July-August). All crop types were completely separable from the others when simultaneously using UAVSAR data spanning the whole growing season. The results demonstrate the feasibility of L-band SAR for crop monitoring and classification, without the need for optical data, and should serve as a guideline for future research.

Keywords: Multi-temporal image; full-polarimetric SAR; crop growth monitoring; polarimetric decomposition; scattering mechanisms; classification.

1. Introduction

Global demand for food is expected to increase in the next 40 years due to continuing growth of the human population and human consumption (Godfray et al., 2010). This increased demand will increase pressure on food production systems, driving the need for agricultural intensification, and in certain areas may increase food insecurity. Monitoring of crop productivity is critical in food security assessment as well as in decision-making in relations to both national and international crop markets (Lal, 2004; Liu et al., 2013). However, it has long been recognized that crop productivity can vary greatly through time, and between agricultural fields, even in small regions (Pinter et al., 2003). As a result, temporally and spatially varying information on plant and soil condition is required to monitor crop productivity. For full season monitoring, this information should be consistent such as to create a time-series across the entire year. Additionally, spatially detailed crop type mapping is also indispensable since most crop yield models are conditional upon specific crops (e.g. Mkhabela et al., 2011).

Remote sensing has been considered as a viable tool for crop mapping and monitoring because of its capability to provide timely and complete coverage over large areas (Jiao et al., 2014). Optical remote sensing is underpinned by two basic physiological processes of vegetation (photosynthesis and evapotranspiration) which can be identified by optical reflectance and temperature parameters. A large body of studies have demonstrated that crops can be characterized only when optical images are available at critical crop growth stages (Blaes et al., 2005; Dong et al., 2015; Skakun et al., 2016). However, these images are often unavailable or incomplete due to rainy weather and frequent cloud cover, particularly over tropical and subtropical regions.

Synthetic aperture radar (SAR) is receiving increasing attention since SAR instruments can acquire data regardless of the weather conditions and cloud cover by operating at wavelengths that can penetrate clouds (Silva et al., 2009; Skriver, 2012). Besides, SAR possesses the capability of capturing crop structural and dielectric properties that differ from the reflectance acquired by optical sensors (McNairn et al., 2009b). The structural characteristics and water content of crops may vary dramatically at different phenological stages, such as the emergence, mature, and senescence stages (Liu et al., 2013). As a consequence, multi-temporal SAR images are commonly used in crop monitoring and classification studies (McNairn et al., 2009b). The main SAR data sources employed by previous crop research involve satellite RADARSAT-1/2 (Choudhury et al., 2006), ENVISAT ASAR (Bouvet et al., 2009), and ALOS PALSAR (McNairn et al., 2009b). However, the majority of these data were restricted to single polarization (e.g. RADARSAT-1) or dual-polarization modes (e.g. ASAR), which greatly limits the practical utility of SAR for crop classification.

When the full-polarimetric SAR data are available, the structure-related scattering mechanisms of crops can be characterized by using polarimetric decomposition parameters (Lee and Pottier, 2009). In fact, there are generally three types of scattering mechanism over agricultural areas; surface scattering, double-bounce scattering, and volume scattering (McNairn et al., 2009b). When the illuminating radar signal arrives at the soil or the upper layer of vegetation canopies, a fraction of the signal is scattered directly by surface scattering. The remaining microwave energy penetrates the crop canopy, and intereacts with the randomly oriented canopy elements, which results in volume scattering. A fraction of the penetrative radar wave interacts with crop stems and surface soil (corner-reflector effects) leading to double-bounce scattering (see illustration in Kwoun and Lu, 2009).

The seasonal patterns of these scattering mechanisms rely heavily on crop type and phenological stages, in which unique information for crop monitoring and identification is potentially provided (e.g. McNairn et al., 2009b; Adams et al., 2013; Jiao et al., 2014; Canisius et al., 2018). Most of these studies were based on C-band SAR thanks to the availability of full-polarimetric RADARSAT-2 data (McNairn and Brisco, 2004). However, the C-band microwave interacts mainly with the upper part of the canopy layer because of its relatively short wavelength (~6 cm) which can hardly penetrate the crop canopy. This results in an early saturation effect, especially for broad leaf crops (Ferrazzoli et al., 1997). Further studies reported low estimation accuracy for crop biophysical parameters (e.g. biomass, leaf area index, and height) with short wavelength (X- or C-band) SAR data (e.g. Paloscia, 2002; Baghdadi et al., 2009).

In contrast, L-band (~20 cm) and P-band (~100 cm) with relatively long wavelength can penetrate into the crop canopy and even reach the surface soil, although the penetration depth depends on the biophysical parameters of the crop canopy (Baghdadi et al., 2009). In theory, crop structure should be better characterized by long wavelengths (L- and P-band) than short wavelengths (X- and C-band). However, there have been very few studies of crop characterization using full-polarimetric L-band SAR (McNairn et al., 2009b; Skriver, 2012; Whelen and Siqueira, 2017), even though some research projects were conducted to collect such data, such as the AgriSAR campaign in Germany (Skriver, 2011) and the Multisensor Airborne Campaign in Italy and Sweden (Macelloni et al., 2001). Research paying special attention to crop monitoring and classification for a wide range of crop types with full year L-band SAR is rare in the literature. It is still not yet fully clear how long wavelength scattering mechanisms for different crop types (especially tree crops), as well as seperability between crops, vary across the growing season. The motivation of this research was, therefore, to fill this knowledge gap by evaluating the potential of time-series L-band full-polarimetric SAR for crop monitoring and classification. The airborne Uninhabited Aerial Vehicle Synthetic Aperture Radar (UAVSAR) data was used in this research.

The major scientific innovations of this research can be summarized as follows:

(1) L-band fully-polarimetric UAVSAR was used for the first time to characterize the seasonal patterns in radar response for tree crops (almond, walnut) as well as other crop types (alfalfa, winter wheat, corn, sunflower, and tomato).

(2) The contributions of scattering mechanisms to radar response were quantified for different crop types, and the seasonal variation in three different scattering mechanisms was analysed.

(3) The separability amongst crop types was assessed and analyzed through the growing season using full calendar year time-series UAVSAR, and this serves as an important guide for future UAVSAR-based crop classification.

The remainder of this paper is organized as follows. In Section 2, the study area is introduced briefly; the methods are described in detail in Section 3; in Section 4, the experimental results are provided; the results are discussed in Section 5; and conclusions are drawn in Section 6.

2. Study area

The study area was focused on an agricultural district stretching over Solano and Yolo counties of California, covering a region about 11 km × 17 km (Fig. 1). The area is located in the middle of the Sacramento Valley, one of the most productive agricultural areas in the United States (Schoups et al., 2005). This region has a typical Mediterranean climate characterized by dry hot summers and wet cool winters (Zhong et al., 2012). Annual precipitation is about 750 mm, mainly concentrated in winter and early spring (Dyer and Rice, 1999). The terrain of the study area is predominantly flat, with relatively deep soil layers. Similar to other areas of the valley, the agricultural systems are complex and heterogeneous. Seven major crop types covering most of the study area were targeted in this research, including almond, walnut, alfalfa, winter wheat, corn, sunflower, and tomato. Each crop has a unique crop calendar with specific seasonal patterns (Pena-Barragan et al., 2011), which provides opportunities to investigate the UAVSAR's potential for monitoring and classification of complex agricultural systems.

Fig. 1 is here

3. Methods

3.1 UAVSAR data and processing

This research employed imagery acquired by the UAVSAR system developed by the NASA Jet Propulsion Laboratory (JPL). UAVSAR is a fully polarimetric L-band SAR designed for monitoring deforming surfaces caused by natural and human activities by using repeat-pass interferometric measurements (Hensley et al., 2009). The frequency of UAVSAR radar is 1.26 GHz, with a wavelength of 23.84 cm, which is long enough to penetrate crop canopies. The radar is mounted onboard a Gulfstream-3 aircraft flown at an altitude of 12.5 km (Chapman et al., 2011), with a 20-km swath and 25°-65° incidence angles. The range and azimuth pixel spacings of the radar are 1.66 and 1 m, respectively. The UAVSAR system provides valuable fine spatial resolution and high-fidelity data with absolute radiometric calibration bias smaller than 1 dB (Fore, 2015), and has been operated over many areas of interest such as North America, Central America, Japan, Greenland and Iceland. The potential of UAVSAR in oil spill detection (Liu et al., 2011), forest characterization (Dickinson et al., 2013), and urban durable changes monitoring (Kim et al., 2016) has been explored extensively.

The UAVSAR data employed in this research were the calibrated and the ground range projected UAVSAR GRD (georeferenced) product, where the covariance matrices are multilook with 3 pixels and 12 pixels in the range and azimuth directions, respectively, producing a spatial resolution of 5 m (Dickinson et al., 2013). The GRD images were extracted with the PolSARpro software developed by the European Space Agency (ESA) (Pottier et al., 2009), and then projected to UTM coordinates with the MapReady software developed by Alaska Satellite Facility (ASF). No further speckle filters were applied since the multiplicative noise (speckle) contained in the SAR images was reduced significantly by the multilook processing (Chapman et al., 2011). A total of nine dates of UAVSAR data through the year 2011 was utilized in this research (Table 1). All flights had nearly identical flight headings and altitude because of the requirement of repeat-pass interferometry (Hensley et al., 2009) which enables direct detection of spatial and temporal variation in radar backscattering coefficients over agricultural fields.

Table 1 is here

3.2 Polarimetric Decomposition Parameters

Polarimetric decomposition is a powerful means of interpreting SAR data in relation to the scattering mechanisms of ground targets. In general, there are two categories of incoherent decomposition methods (Eigenvalue-eigenvector-based and model-based) which are considered suitable for characterizing the scattering behaviour of natural targets (Lee and Pottier, 2009). In this research, the Cloude–Pottier (CP) and Freeman-Durden (FD) decompositions were performed on each UAVSAR dataset with the PolSARpro software (Pottier et al., 2009).

The CP decomposition describes the strength of scattering mechanism with eigenvectors and eigenvalues (Cloude and Pottier, 1997). Three parameters are usually derived from CP decomposition; entropy (H), anisotropy (A) and alpha angle (α). For each pixel of an image, entropy ranging between 0 and 1 quantifies the randomness of scattering. Low entropy signifies the domination of a single scattering mechanism, and high entropy suggests the occurrence of more than one scattering mechanism; in the extreme case when H =1, the target scattering becomes a random noise process without any polarization information. Alpha angle (0-90°) can be used to determine the primary scattering. With medium entropy (0.5-0.9), alpha angle values smaller than 40°, around 45° and larger than 50° indicate the dominance of surface scattering (e.g. smooth land surfaces), dipole or volume scattering (e.g. vegetation canopies), and double-bounce scattering (e.g. forests), respectively (Cloude and Pottier, 1997). Anisotropy measures the relative strength between the secondary and third scattering mechanisms; a large value suggests the occurrence of only one powerful secondary scattering mechanism, while a small value shows the contribution of a third scattering process. The FD decomposition is a model-based technique, based on which the respective strength of single-bounce

(Odd), double-bounce (Dbl), and volume (Vol) scatters for each target (pixel) can be determined (Freeman and Durden, 1998). The three fractions are respectively modeled by scattering from a first order Bragg surface, a dihedral corner reflector (e.g. ground-tree trunk backscatter), and randomly oriented thin cylindrical dipoles (e.g. forest canopy).

3.3 Ground reference data

Timely field survey over the study area was not possible since the UAVSAR data were collected in 2011. The United States Department of Agriculture (USDA) Cropland Data Layer (CDL) was, thus, employed to identify crop types and acquire ground reference data (USDA-NASS, 2011 (b)). The CDL has already been used in a variety of remotely sensed crop applications (e.g. Zheng et al., 2015; Whelen and Siqueira, 2017) due to its very high quality (Boryan et al., 2011). It is produced annually with several types of moderate spatial resolution optical imagery and a large amount of ground reference data by using a supervised decision tree classification approach (Boryan et al., 2011). The overall classification accuracy of CDL is reported at the state level; 83% for the major crops in California in 2011. The accuracies for the seven crops analyzed in this study were reasonable, ranging from 75.7% (walnut) to 93.5% (alfalfa and tomato). By visual inspection we found that misclassified pixels of CDL were mainly concentrated at the edge of crop fields such that it was possible to identify reliably a crop class if a field was dominated by a single class according to the CDL.

Fig. 2 is here

The process of field reference data labeling consisted of three steps. First, the UAVSAR image in July (with clear crop field boundaries) was overlaid on the projected CDL image (with UTM coordinate); to acquire representative samples, crop fields shown in the UAVSAR image with area larger than 5 ha were identified according to the CDL. Second, each identified crop field was outlined manually and buffered inwardly from the field boundary by one pixel (Whelen and Siqueira, 2017), so that the centre of the field could be targeted for sampling; the average size of fields varied among crop types due to their different surface characteristics (Fig. 2). Third, the outlined field patches belonging to the same crop were merged to comprise a stratum, and several samples (pixels) were generated randomly within each stratum; the number of samples in each category was made proportional to its area. A total of 1438 samples were acquried finally, including 70 for almond, 110 for walnut, 319 for alfalfa, 340 for winter wheat, 99 for corn, 170 for sunflower, and 330 for tomato.

3.4 Separability between crop types

The Jeffries–Matusita (JM) distance, an indicator of the average distance between two class density functions, was employed to assess quantitatively the between-class separability (Richards and Jia, 1999). The JM distance, taking both first order (mean) and second order (variance) of samples into consideration, has been demonstrated to be an ideal distance measure for multi-dimensional remotely sensed data (e.g. Schmidt and Skidmore, 2003; Laurin et al., 2013). Under normality assumpitions, the JM distance between a pair of classes (l and k) can be calculated with the following equation:

$$\mathrm{JM} = 2(1 - e^{-B}) \tag{1}$$

in which the Bhattacharyya (B) distance is defined as:

$$B = \frac{1}{8}(\mu_l - \mu_k)^T \left(\frac{\Sigma_l + \Sigma_k}{2}\right)^{-1} (\mu_l - \mu_k) + \frac{1}{2}\ln\left(\frac{|(\Sigma_l + \Sigma_k)/2|}{\sqrt{|\Sigma_l||\Sigma_k|}}\right) \quad (2)$$

where μ_l and μ_k are the mean vectors of classes l and k, respectively, and $\sum_l$ and $\sum_k$ are the corresponding covariance matrices.

The JM distance ranges between 0 and 2, with a larger value suggesting a greater average distance between a pair of classes. Laurin et al. (2013) suggested that a value of 1.9 indicates good separability. The JM distance is asymptotic to 2.0, which indicates the between-class difference being larger than the within-class difference. That is, the image classification accuracy is nearly perfect if only two classes are considered (Richards and Jia, 1999).

In this research, the JM distance was investigated for all pairs of crops with each UAVSAR image to explore how that separability varied throughout the year. In addition, the growing season JM distances for each pair of crop types were also examined to determine the extent to which crop separability can be increased using multitemporal images. The growing season in this analysis denotes the period from March to October, which covers the phenological growth stages of crops.

4. Results

4.1 Spatial and temporal variation in radar backscattering value

The average backscattering values in the three linear polarizations (HH, HV, and VV) for each crop during the growing season were calculated and are shown in Fig. 3. In general, the seasonal patterns of each crop were similar across the polarizations. Specifically, the patterns were more explicit in the cross-polarized HV polarization than in the co-polarized HH and VV polarizations. Taking sunflower as an example, the amplitude of variation was about 18 dB in HV, while only approximately 13 dB in HH and VV. These results are in accordance with previous studies, which have reported that cross-polarized (HV or VH) data are sensitive to crop phenological stages (e.g. Liu et al., 2013; Whelen and Siqueira, 2017; Canisius et al., 2018). As a result, we focused on the HV polarization as a proxy in the following analysis of variation in radar backscattering.

Figs. 3 and 4 are here

Drawing on official statistics (California Agricultural Statistics, 2011; USDA-NASA, 2011 (a)), calendars of the studied crops are summarized in Fig. 4. Almond and walnut are perennial tree crops which usually bloom and leaf out in spring and senesce in autumn, with woody structures during the dormancy period (Pena-Barragan et al., 2011). The HV backscattering values for the two tree crops were both very large and stable (around -15 dB) during the whole year. Alfalfa is also a perennial crop that starts growth in early spring and senescence in late autumn (Fig. 4). The backscattering values for alfalfa were also relatively constant but small (about -30 dB), with fluctuations across the growing season that can be attributed to yearly cutting activities (Zhong et al., 2012). In contrast, phenological stages for winter wheat and summer crops are shown clearly in the HV profile. Winter wheat is usually germinated from late September through to the next January, during which small HV values were sustained (Fig. 3); it resumes growth in spring when the weather is warmer, as indicated by the increase from January to March; it then senesces and is harvested from early May to late July, exhibited by the continuing decrease in HV (-15 dB to -22 dB) during this period. For the summer crops, they are planted and emerge in spring (early March to late May) and reach peak biomass in July. This was captured by the rapid increase in HV values (-33 dB to about -20 dB) during the period. The senescence stage lasts from late July to late November with large difference between corn and the other crops (sunflower and tomato) (Fig. 3). The earlier senescence and harvest for sunflower and tomato was depicted by the earlier HV decline from late July to early October, while corn maintained a large HV value (-20 dB) during July-August and then began to decrease until late November.

Fig. 5 is here

It should be noted that the calendar for the same crop may vary between different areas due to natural conditions (e.g. weather conditions, soil water content, and field slope) and farmer decisions (Saich and Borgeaud, 2000). To demonstrate such variation clearly, the standard deviation (STD) profile of the HV polarization signatures for each crop are shown in Fig. 3(d). Seasonal patterns of STD for the permanent crops (i.e. almond, walnut, and alfalfa) are comparable and relatively stable (about 2~4 dB), with a general downward trend over the growing season. Winter wheat had small STD values (below 3 dB) during January-to-May, but relatively large values (over 3.5 dB) during June-to-October, which might be attributable to the second planting of some harvested fields. As for the summer crops, two STD peaks (generally > 5 dB) were conspicuous in the profiles. The first occurred during June, caused by the difference in growth time amongst crops, while the second occurred during October, caused by the difference in harvesting time (Figs. 3(d) and 4). To highlight such field-to-field spatial variation, the HV polarization during the growing season (March to October) is shown in Fig. 5, in which typical fields for each crop are marked by black patches. In general, the results were consistent with the analysis of the STD in the HV polarization. That is, the radar signature of crops was heterogeneous in the June and October images, but homogeneous in the images dated March, May, July and August.

4.2 Characterization of scattering mechanisms for crops

The CP decomposition can determine the dominant scattering of land surface targets via the entropy-alpha angle feature plane (Cloude and Pottier, 1997). Progressions of entropy (H), anisotropy (A), and alpha angle (α) for the crops are depicted in Fig. 6. The entropy, denoting the randomness of scattering, was rather large and stable for the two tree crops (> 0.8) and alfalfa (around 0.7) during the growing season. This implies the occurance of multiple scattering mechanisms. The entropy for the non-permanent crops (winter wheat and summer crops) increased rapidly from emergence (about 0.45) to ripening stage (around 0.7), and then decreased sharply during the harvest stage (Fig. 6). Alpha angle, discerning the primary scattering mechanisms, was distributed in the range of 35°-50° for the three perennial crops throughout the observation period. This indicates the large contribution of dipole scattering to radar response. However, the value for the two tree crops during the leaf-on season (March to October) was smaller than that during the leaf-off season (October to the next March). This suggests that dipole scattering was attenuated with the presence of leaves. For winter wheat and summer crops, the seasonal patterns of alpha angle resemble those of entropy. That is, alpha angle increased with the growth of crops and then decreased during the senescence stage. The relatively small value (16°-32°) during the non-growing season (July to December for winter wheat, and November to the next May for the summer crops) indicates that surface scattering from soil was the dominant scattering mechanism. The anisotropy can be most useful when $H >$ 0.7, when heavily affected by noise with low entropy (Lee and Pottier, 2009). A consistently small anisotropy (<0.6) was found for the two tree crops and summer crops through the growing season, suggesting comparable strength of the secondary and third scattering processes. In contrast, alfalfa had a relatively large value (>0.6) compared the other crops across the observation period, implying the presence of a strong secondary scattering mechanism. However, it is not possible to provide a definitive interpretation of the scattering mechanism.

Figs. 6 and 7 are here

In comparison, the relative strength of scattering mechanisms can be interpreted straightforwardly with the proportional (%) report of scattering contributions provided by the FD decomposition (Fig. 7). All three scattering processes contributed to the radar response of the crops. However, their proportional contributions vary considerably for each crop during the growing season. For the two tree crops, volume scattering was identified as the greatest contribution (>40%) throughout the year. It is noticable that the contribution of surface scattering during May-to-October (with dense leaves) was larger by about 10 % than that during October to the next May, while the contribution of double-bounce scattering behaved in the opposite manner. In contrast, surface scattering dominated for alfalfa, with a contribution larger than 40% across the year. However, in comparison with the other crops, a large contribution (>30%) of double-bounce scattering was observed during March-to-September, about 10% larger than that of volume scattering (Fig. 7). This explains why the anisotropy for alfalfa was large during this period (Fig. 6(b)). Surface scattering was clearly dominant (>50%) for winter wheat through the year although the contributions of volume and double-bounce scattering were also high during March (30%). Similarly, surface scattering (>60%) also dominated for summer crops over most of the year although volume scattering was identified as the primary scattering mechanism (>40%) for sunflower and tomato during June and for corn during July-to-October.

4.3 Separability assessment between crops

The mean JM distances for each crop to the other crops across the year with linear polarizations and decomposition (CP and FD) parameters were calculated and are shown in Fig. 8. In general, the CP and FD parameters provided greater spearability (with larger JM values) than the linear polarizations. Taking the mean distance from tomato to the other crops during August as an example, the JM value increased from 1.1 with linear polarizations to over 1.4 with both the CP and FD decomposition parameters (Fig. 8). Similar JM variation patterns were observed for each crop over the three datasets. Two tree crops were clearly discernible from October to the next May when summer crops were not yet emerged. Winter wheat was most separable during spring (March through May) and summer (July and August) due to its exclusive calendar. Alfalfa and summer crops had the greatest separability during the period from July to August. In general, the greatest separability between crops occurred during July-to-August and March, although the mean JM for most of crops was less than 1.6. In contrast, the separability was low during the period from October to the next January as well as June. The combined use of linear polarizations and decomposition parameters (CP and FD) considerably increased the separability between crops over the year, with most of JM values greater than 1.5. As expected, the greatest separability occured during the summer (July-to-August) when most JM distances were larger than 1.8. It must be noted that the largest increase in separability was observed during June, when all of the JM values increased to relatively large values (>1.5).

Fig. 8 is here

The separability was found to vary over the growing season (March to October) due to the specific calendars and structures of crops. To evaluate the benefit of using multi-temporal imagery for crop monitoring and classification, JM distances for all crop type pairs with growing seasonal linear polarizations, CP parameters, FD parameters, and all available bands (combination of linear polarizations and CP and FD parameters) were calculated and listed in Table 2. It is clear that the two tree crops could be easily discriminated (JM = 2) from the other crops with linear polarizations due to their unique physical characteristics. However, the two crops themselves were hard to separate (JM=1.747). Similarly, alfalfa and winter wheat were also highly separable from the other crops (JM > 1.99), with low discrimination between the two crops (JM =1.845). The separability between summer crops was also low because of their similar calendars (Fig. 4). Amongst the three crops, the separability between corn and sunflower was the greatest (JM = 1.959) while that between sunflower and tomato was the least (JM < 1.711). As expected, the discrimination between crops was clearly increased (i.e. larger JM values) with the CP and FD parameters, especially for those indiscernible crop pairs (e.g. almond-walnut, alfalfa-winter wheat, sunflower-tomato). For example, the JM distance between almond and walnut was larger than 1.96 with the CP and FD parameters. It should be noted that each crop was completely separable from the others (JM = 2 for each pair of crops) if all avaiblable bands were considered (Table 2).

Tables 2 and 3 are here

To further validate the potential of UAVSAR in crop discrimination, two machine learning algorithms, the Multi-layer Perceptron (MLP) and Support Vector Machine

(SVM), were employed using different features (linear polarizations and polarimetric parameters). The control parameters of the MLP were set by following the recommendations of Zhang et al. (2018). The most suitable radial basis function (RBF) kernel SVM was used in this research, with the parameters being optimized through a grid search method with five-fold cross validation (Barrett et al., 2014). Table 3 summarizes the classification accuracy assessment, including the overall accuracy (OA) and Kappa coefficient (*k*). The OA and *k* produced by different features using both algorithms were in accordance with the analysis of JM distance. As shown in Table 3, the CP and FD decomposition parameters produced consistently greater accuracy in comparison to the linear polarizations, with OA = 93.01% and 93.71% by MLP, and OA = 92.03% and 93.01% by SVM, respectively; the combined use of all features (linear polarizations and polarimetric parameters) achieved the largest classification OA, with up to 95.80% using MLP and 97.48% using SVM, respectively. Such coherency of classification accuracy further supports the analysis of JM distance, and demonstrates the unique value of polarimetric parameters in SAR-based crop classification.

5. Discussion

Over vegetated crop fields, emitted radar energy is attenuated by crop vegetation as well as land surface soil. The amount of radar energy that is scattered back to the antenna is related directly to the structural characteristics (e.g. size, shape, density, orientation) as well as SAR system parameters, such as polarization, incidence angle, and wavelength (Saich and Borgeaud, 2000; Kwoun and Lu, 2009). In the full-polarimetric polarization mode, three linear polarizations (HH, HV, and VV) are simultaneously collected. In general, horizontally polarized waves (H) can penetrate vegetation canopies better than vertically polarized waves (V), and the HH polarization, thus, tends to characterize surface soil condition (Lin and Sarabandi, 1999). In contrast, vertically polarized waves are sensitive to vertical vegetation structure, and the VV polarization, thus, provides more information about vertical structural characteristics. The cross polarization (HV or VH) measures multiple-scattering from the soil surface and vegetation volume and is, thus, sensitive to crop structure within the total canopy volume. This explains why the HV polarization was more sensitive to crop growth than the HH and VV polarizations in this research (Fig. 3). The results are in line with previous reports (e.g. Jiao et al., 2014; Canisius et al., 2018).

It was found that the radar responses of perennial crops (almond, walnut, and alfalfa) were relatively stable across the growing season. This suggests that the woody structure or herbaceous stems rather than leaves are responsible for their radar responses. In contrast, the responses increased rapidly for winter wheat and summer crops from the emergence stage to the peak biomass stage since their structural characteristics varied markedly with crop growth. However, it is visible that seasonal backscattering values of the summer crops were generally greater than those of winter wheat (Fig. 3), which is consistent with the reports by Liu et al. (2013) and Whelen and Siqueira (2017). This can be attributed to the difference in biomass between winter wheat (thin stems with narrow leaves) and summer crops (thick stems with broad leaves) (Macelloni et al., 2001).

Previous studies pointed out that radar signatures of surface targets depend on incidence angle (Skriver et al., 1999). However, it has been demonstrated that this dependence becomes relatively weak with crop growth (Saich and Borgeaud, 2000; Liu et al., 2013). In addition, the study area covered in this research is relatively small, and variation in incidence angle should be limited. It is, therefore, likely that the effect of incidence angle on crop signatures was minimal in this research. Weather conditions (e.g. precipitation and freezing) may also affect radar signatures. The soil reflectance is a large component of the radar response, especially when soil has not yet been fully covered by the crop canopy. The presence of precipitation will raise the soil conductivity and, hence, increase considerably the intensity of radar response. Fortunately, nearly all the employed UAVSAR images were acquired under dry conditions (Table 1). Freezing in the soil might decrease the dielectric constant of soil/vegetation (reduction in liquid water), and hence decrease the radar response (Saich and Borgeaud, 2000). We note that the minimum air temperatures for the January and December images were around freezing point. However, given the very small amounts of rainfall on the image acquisition dates and in the few days preceding them (data not shown) we believe that the effect of freezing on the observed crop radar signatures was negligible.

The scattering mechanisms of crops characterized by the CP and FD decompositions were generally comparable, and some interesting results were observed. The dominant volume scattering, as well as double-bounce scattering for the two tree crops, was attenuated during May-to-October, when the surface scattering was enhanced. This is because as the tree crops grow and become denser, less microwave energy can penetrate their canopies and more radar signal was, thus, scattered on the smooth uppermost canopies (Huang et al., 2017). This can also explain why the greatest contributions of volume scattering, and double-bounce scattering for sunflower and tomato, occurred during June (Figs. 6 and 7), rather than during the peak biomass stage with denser leaves (July and August). In comparison with the dense structure (crowded and horizontally oriented leaves) of sunflower and tomato, corn has sparse and randomly oriented leaves (Fig. 9) which exert less impact on the penetration of the radar signal, even during the peak biomass stage. As a result, as the corn grew taller and denser (July-to-October), volume scattering became dominant, as depicted in Fig. 7. This difference in dominant scattering should be very useful for separation of corn from other summer crops. It is also notable that the double-bounce scattering for alfalfa remained consistently large (over 30%) during the growing season, indicating that the L-band microwave could easily penetrate the alfalfa's narrow-leafed canopies. This unique signature might be further explored to identify alfalfa by using SAR data without training samples. In contrast, the contribution of volume scattering for alfalfa was generally smaller than for the other crops, which might be attributable to the small amount of biomass.

The JM distance-based assessment presented here further indicates that polarimetric decomposition parameters provided greater separability for crop discrimination than linear polarizations, which agrees with the reports by McNairn et al. (2009b) for ALOS PALSAR and by Li et al. (2012) for RADARSAT-2 data. This may be attributed to the fact that polarimetric decomposition parameters can characterize the unique biophysical properties of crops (e.g. plant height) more closely than linear polarizations (Canisius et al., 2018), which is valuable for crop discrimination (McNairn et al., 2009b). It is interesting to note that the least separability across the growing season (March-October) occured during June and October. This is in line with a previous study by Skriver (2012) who also reported a small classificaiont accuracy with airborne SAR data in June. In fact, for a certain crop the green-up onset date, as well as senescence date, may vary greatly over crop fields due to soil and topographic conditions, and farm decisions (Fig. 5), leading to great regional intra-class variation in polarimetric signatures (Fig. 3(d)). This might explain why crop discrimination was low for the June and October images.

6. Summary and conclusions

This paper evaluated the applicability of L-band full-polarimetric UAVSAR SAR data for crop monitoring and classification over an agricultural area in the California's Sacramento Valley. The structure-related and phenology-driven polarimetric signature of each crop was provided by multi-temporal UAVSAR data, with a fine temporal resolution. The cross-polarized band (HV) was found to be more sensitive to crop growth than the co-polarized bands (HH and VV). Tree crops (almond and walnut) had the largest radar response because of their large volume of canopies, followed by broad-leafed summer crops (corn, sunflower, and tomato), while narrow-leafed winter wheat and alfalfa had the smallest response. Prominent regional intra-class variation occurred during June and October, because of the differences in green-up onset date as well as senescence date between crop fields. In contrast, the signature over intra-class fields was homogeneous during the peak biomass stage (July and August).

The structural characteristics of crops were well characterized by their unique scattering patterns with the parameters derived from the Cloude-Pottier (CP) and Freeman-Durden (FD) decompositions. The predominant mechanism for the tree crops was volume scattering, which accounts for over 40% of the radar response through the year. In contrast, surface scattering was dominant (>40%) for the narrow-leafed alfalfa and winter wheat crops, although double-bounce scattering (~30%) for alfalfa was also notable. Surface scattering was also dominant (>40%) for summer crops over most of the year except for sunflower and tomato during June and corn during July-to-October when volume scattering was identified as the primary scattering mechanism. The difference in seasonal patterns of scattering mechanisms among crops provides valuable information for crop classification.

The separability assessment indicated that crops were much more separable with the CP or FD decomposition parameters than with the linear polarizations. The separability between crops varied greatly over the growing season, and the largest separability generally occurred during the peak biomass stage (July and August) with the least during June and October. The combined use of linear polarizations and CP and FD decomposition parameters significantly increased crop discrimination through the year, suggesting complementary information had been provided. It is notable that all crop types were completely separable from the other crops by simultaneously using UAVSAR data spanning the growing season.

This paper illustrated the potential of time-series UAVSAR data for crop growth monitoring and classification. Our results indicated that very high accuracy crop mapping can be expected based solely on time-series UAVSAR, which will be a priority for future research. This research emphasized the unique value of polarimetric decomposition parameters for crop discrimination and classification. Future research will also focus on employing these physically meaningful parameters to retrieve crop biophysical parameters (e.g. height, biomass, and leaf area index), which are critical for crop yield estimation as well as crop management.

Acknowledgements

This research was co-funded by the Jilin Province Science and Technology Development Program (20170520087JH, 20170204025SF), the National Key Research and Development Program of China (2017YFB0503602), and the National Natural Science Foundation of China (41301465, 41671397). We would like to thank the support from China Scholarship Council (CSC) (File No. 201704910192) during a visit of Huapeng Li to Lancaster Univerisity. We also thank Alaska Satellite Facility for the supply of UAVSAR data employed in this research.

References

Adams, J.R., Rowlandson, T.L., McKeown, S.J., Berg, A.A., McNairn, H., Sweeney, S.J., 2013. Evaluating the Cloude-Pottier and Freeman-Durden scattering decompositions for distinguishing between unharvested and post-harvest agricultural fields. Can. J. Remote Sens. 39 (4), 318-327.

Baghdadi, N., Boyer, N., Todoroff, P., El Hajj, M., Begue, A., 2009. Potential of SAR sensors TerraSAR-X, ASAR/ENVISAT and PALSAR/ALOS for monitoring sugarcane crops on Reunion Island. Remote Sens. Environ. 113 (8), 1724-1738.

Barrett, B., Nitze, I., Green, S., Cawkwell, F., 2014. Assessment of multi-temporal, multi-sensor radar and ancillary spatial data for grasslands monitoring in Ireland using machine learning approaches. Remote Sens. Environ. 152 (6), 109-124.

Blaes, X., Vanhalle, L., Defourny, P., 2005. Efficiency of crop identification based on optical and SAR image time series. Remote Sens. Environ. 96 (3-4), 352-365.

Boryan, C., Yang, Z.W., Mueller, R., Craig, M., 2011. Monitoring US agriculture: the US Department of Agriculture, National Agricultural Statistics Service, Cropland Data Layer Program. Geocarto Int. 26 (5), 341-358.

Bouvet, A., Le Toan, T., Lam-Dao, N., 2009. Monitoring of the Rice Cropping System in the Mekong Delta Using ENVISAT/ASAR Dual Polarization Data. IEEE Trans. Geosci. Remote Sens. 47 (2), 517-526.

California Agricultural Statistic, 2011. USDA's National Agricultural Statistics Service, California Field Office. Retrieved February 3, 2018, from. www.nass.usda.gov/ca.

Canisius, F., Shang, J., Liu, J., Huang, X., Ma, B., Jiao, X., Geng, X., Kovacs, J.M., Walters, D., 2018. Tracking Crop Phenological Development Using Multi-temporal Polarimetric Radarsat-2 Data. Remote Sens. Environ. 210 (6), 508-518.

Chapman, B., Hensley, S., Lou, Y., 2011. The JPL UAVSAR. ASF News & Notes. 7(1) Retrieved from. https://www.asf.alaska.edu/news-notes/7-1/jpl-uavsar/.

Choudhury, I., Chakraborty, M., 2006. SAR signature investigation of rice crop using RADARSAT data. Int. J. Remote Sens. 27 (3), 519-534.

Cloude, S.R., Pottier, E., 1997. An entropy based classification scheme for land applications of polarimetric SAR. IEEE Trans. Geosci. Remote Sens. 35 (1), 68-78.

Dickinson, C., Siqueira, P., Clewley, D., Lucas, R., 2013. Classification of forest composition using polarimetric decomposition in multiple landscapes. Remote Sens. Environ. 131 (6), 206-214.

Dong, J., Xiao, X., Kou, W., Qin, Y., Zhang, G., Li, L., Jin, C., Zhou, Y., Wang, J., Biradar, C., Liu, J., Moore Iii, B., 2015. Tracking the dynamics of paddy rice planting area in 1986–2010 through time series Landsat images and phenology-based algorithms. Remote Sens. Environ. 160 (4), 99-113.

Dyer, A.R., Rice, K.J., 1999. Effects of competition on resource availability and growth of a California bunchgrass. Ecology. 80 (8), 2697-2710.

Ferrazzoli, P., Paloscia, S., Pampaloni, P., Schiavon, G., Sigismondi, S., Solimini, D., 1997. The potential of multifrequency polarimetric SAR in assessing agricultural and arboreous biomass. IEEE Trans. Geosci. Remote Sens. 35 (1), 5-17.

Fore, A.G., Chapman, B.D., Hawkins, B.P., Hensley, S., Jones, C.E., Michel, T.R., Muellerschoen, R.J., 2015. UAVSAR Polarimetric Calibration. IEEE Trans. Geosci. Remote Sens. 53 (6), 3481-3491.

Freeman, A., Durden, S.L., 1998. A three-component scattering model for polarimetric SAR data. IEEE Trans. Geosci. Remote Sens. 36 (3), 963-973.

Godfray, H.C.J., Beddington, J.R., Crute, I.R., Haddad, L., Lawrence, D., Muir, J.F., Pretty, J., Robinson, S., Thomas, S.M., Toulmin, C., 2010. Food Security: The Challenge of Feeding 9 Billion People. Science. 327 (5967), 812-818.

Hensley, S., Zebker, H., Jones, C., Michel, T., Muellerschoen, R., Chapman, B., 2009. First deformation results using the NASA/JPL UAVSAR instrument. 2nd Asian-Pacific Conference on Synthetic Aperture Radar (pp. 1051-1055). Xi'an Shanxi, China: IEEE.

Huang, X.D., Wang, J.F., Shang, J.A., Liao, C.H., Liu, J.G., 2017. Application of polarization signature to land cover scattering mechanism analysis and classification using multi-temporal C-band polarimetric RADARSAT-2 imagery. Remote Sens. Environ. 193 (5), 11-28.

Jiao, X.F., Kovacs, J.M., Shang, J.L., McNairn, H., Walters, D., Ma, B.L., Geng, X.Y., 2014. Object-oriented crop mapping and monitoring using multi-temporal polarimetric RADARSAT-2 data. ISPRS J. Photogramm. Remote Sens. 96 (10), 38-46.

Kim, D.J., Hensley, S., Yun, S.H., Neumann, M., 2016. Detection of Durable and Permanent Changes in Urban Areas Using Multitemporal Polarimetric UAVSAR Data. IEEE Trans. Geosci. Remote Sens. 13 (2), 267-271.

Kwoun, O.I., Lu, Z., 2009. Multi-temporal RADARSAT-1 and ERS Backscattering Signatures of Coastal Wetlands in Southeastern Louisiana. Photogrammetric Engineering and Remote Sensing 75 (5), 607-617.

Lal, R., 2004. Soil carbon sequestration impacts on global climate change and food security. Science. 304 (5677), 1623-1627.

Laurin, G.V., Del Frate, F., Pasolli, L., Notarnicola, C., Guerriero, L., Valentini, R., 2013. Discrimination of vegetation types in alpine sites with ALOS PALSAR-, RADARSAT-2-, and lidar-derived information. Int. J. Remote Sens. 34 (19), 6898-6913.

Lee, J. S., Pottier, E., 2009. Polarimetric radar imaging from basics to applications. New York: CRC Press.

Li, K., Brisco, B., Shao, Y., Touzi, R., 2012. Polarimetric decomposition with RADARSAT-2 for rice mapping and monitoring. Can. J. Remote Sens. 38 (2), 169-179.

Lin, Y.C., Sarabandi, K., 1999. A Monte Carlo coherent scattering model for forest canopies using fractal-generated trees. IEEE Trans. Geosci. Remote Sens. 37 (1), 440-451.

Liu, C., Shang, J.L., Vachon, P.W., McNairn, H., 2013. Multiyear Crop Monitoring Using Polarimetric

RADARSAT-2 Data. IEEE Trans. Geosci. Remote Sens. 51 (4), 2227-2240.

Liu, P., Li, X.F., Qu, J.J., Wang, W.G., Zhao, C.F., Pichel, W., 2011. Oil spill detection with fully polarimetric UAVSAR data. Marine Pollution Bull. 62 (12), 2611-2618.

Macelloni, G., Paloscia, S., Pampaloni, P., Marliani, F., Gai, M., 2001. The relationship between the backscattering coefficient and the biomass of narrow and broad leaf crops. IEEE Trans. Geosci. Remote Sens. 39 (4), 873-884.

McNairn, H., Brisco, B., 2004. The application of C-band polarimetric SAR for agriculture: a review. Can. J. Remote. Sens. 30 (3), 525-542.

McNairn, H., Champagne, C., Shang, J., Holmstrom, D., Reichert, G., 2009a. Integration of optical and Synthetic Aperture Radar (SAR) imagery for delivering operational annual crop inventories. ISPRS J. Photogram. Rem. Sens. 64 (5), 434-449.

McNairn, H., Shang, J.L., Jiao, X.F., Champagne, C., 2009b. The Contribution of ALOS PALSAR Multipolarization and Polarimetric Data to Crop Classification. IEEE Trans. Geosci. Remote Sens. 47 (12), 3981-3992.

Mkhabela, M.S., Bullock, P., Raj, S., Wang, S., Yang, Y., 2011. Crop yield forecasting on the Canadian Prairies using MODIS NDVI data. Agric. Forest Meteorol. 151 (3), 385-393.

National Oceanic and Atmospheric Administration, National Centers for Environmental Information (NOAA-NCEI), 2011. Local Climatological Data (LCD), Sacramento Executive Airport, Sacramento County, CA. National Environmental Satellite, Data, and Information Service. Retrieved February 3, 2018, from. https://www.ncdc.noaa.gov/cdo-web/datasets/LCD/stations/WBAN:23232/detail.

Paloscia, S., 2002. A summary of experimental results to assess the contribution of SAR for mapping vegetation biomass and soil moisture. Can. J. Remote Sens. 28 (2), 246-261.

Pena-Barragan, J.M., Ngugi, M.K., Plant, R.E., Six, J., 2011. Object-based crop identification using multiple vegetation indices, textural features and crop phenology. Remote Sens. Environ. 115 (6), 1301-1316.

Pinter, P.J., Hatfield, J.L., Schepers, J.S., Barnes, E.M., Moran, M.S., Daughtry, C.S.T., Upchurch, D.R., 2003. Remote sensing for crop management. Photogram. Eng. Remote Sens. 69 (6), 647-664.

Pottier, E., Ferro-Famil, L., Allain, S., Cloude, S., Hajnsek, I., Papathanassiou, K., Moreira, A., Williams, M., Minchella, A., Lavalle, M., Desnos, Y.L., 2009. Overview of the PolSARpro V4.0 software: the open source toolbox for polarimetric and interferometric polarimetric SAR data processing. In: Proceedings of 2009 IEEE International Geoscience and Remote Sensing Symposium, Cape Town, South Africa, July 12-17, vol. 4, pp. 936-939.

Richards, J. A., Jia, X., 1999. Remote sensing digital image analysis, an introduction. 3rd, revised and enlarged ed. Berlin: Springer-Verlag.

Saich, P., Borgeaud, M., 2000. Interpreting ERS SAR signatures of agricultural crops in Flevoland, 1993-1996. IEEE Trans. Geosci. Remote Sens. 38 (2), 651-657.

Schmidt, K.S., Skidmore, A.K., 2003. Spectral discrimination of vegetation types in a coastal wetland. Remote Sens. Environ. 85 (1), 92-108.

Schoups, G., Hopmans, J.W., Young, C.A., Vrugt, J.A., Wallender, W.W., Tanji, K.K., Panday, S., 2005.

Sustainability of irrigated agriculture in the San Joaquin Valley, California. Proc. Natl. Acad. Sci. U.S.A. 102 (43), 15352-15356.

Silva, W.F., Rudorff, B.F.T., Formaggio, A.R., Paradella, W.R., Mura, J.C., 2009. Discrimination of agricultural crops in a tropical semi-arid region of Brazil based on L-band polarimetric airborne SAR data. ISPRS J. Photogram. Rem. Sens. 64 (5), 458-463.

Skakun, S., Kussul, N., Shelestov, A.Y., Lavreniuk, M., Kussul, O., 2016. Efficiency Assessment of Multitemporal C-Band Radarsat-2 Intensity and Landsat-8 Surface Reflectance Satellite Imagery for Crop Classification in Ukraine. IEEE J. Selected Topics Appl. Earth Observ. Remote Sens. 9 (8), 3712-3719.

Skriver, H., 2012. Crop Classification by Multitemporal C- and L-Band Single- and Dual-Polarization and Fully Polarimetric SAR. IEEE Trans. Geosci. Remote Sens. 50 (6), 2138-2149.

Skriver, H., Svendsen, M.T., Thomsen, A.G., 1999. Multitemporal C- and L-band polarimetric signatures of crops. IEEE Trans. Geosci. Remote Sens. 37 (5), 2413-2429.

USDA NASS, 2011 (a). Crop Progress. Retrieved January 13, 2018, from. http://usda.mannlib.cornell.edu/MannUsda/viewDocumentInfo.do;jsessionid=A8F0A37CA76B0F6E77E0FDE1E10BA5F9?documentID=1048/.

USDA NASS, 2011 (b). National Agricultural Statistics Service Cropland Data Layer. Retrieved January 13, 2018, from. http://nassgeodata.gmu.edu/CropScape/.

Whelen, T., Siqueira, P., 2017. Use of time-series L-band UAVSAR data for the classification of agricultural fields in the San Joaquin Valley. Remote Sens. Environ. 193 (5), 216-224.

Zhang, C., Pan, X., Li, H.P., Gardiner, A., Sargent, I., Hare, J., Atkinson, P.M., 2018. A hybrid MLP-CNN classifier for very fine resolution remotely sensed image classification. ISPRS J. Photogram. Rem. Sens. 140 (6), 133-144.

Zheng, B.J., Myint, S.W., Thenkabail, P.S., Aggarwal, R.M., 2015. A support vector machine to identify irrigated crop types using time-series Landsat NDVI data. Int. J. Appl. Earth Obs. Geoinf. 34 (1), 103-112.

Zhong, L.H., Gong, P., Biging, G.S., 2012. Phenology-based Crop Classification Algorithm and its Implications on Agricultural Water Use Assessments in California's Central Valley. Photogram. Eng. Remote Sens. 78 (8), 799-813.

Figure Captions

Fig. 1. The study site in the agricultural region of the Sacramento Valley, California.

Fig. 2. (a) The UAVSAR image dated 20 July, 2011 (R-G-B, bands VV, HV, and HH), (b) the outlined crop fields.

Fig. 3. Temporal variation in average backscattering values for crops over linear polarizations (a) HH, (b) HV, (c) VV; Note error bars denote standard deviation. (d) standard deviation profile with HV polarization was depicted separately for analysis.

Fig. 4. Crop calendar for the seven major crops in the study area. Note there is no planting time for the perennial almond, walnut, and alfalfa crops.

Fig. 5. Radar backscattering values (HV polarization) shown in the UAVSAR images dated (a) 30 March (b) 12 May, (c) 16 June, (d) 20 July, (e) 29 August, and (f) 03 October. Note typical fields for the studied crops were marked by black patches.

Fig. 6. Time-series variation in average (a) entropy, (b) anisotropy, and (c) alpha angle derived from the Cloude-Pottier decomposition. Note error bars denote standard deviation.

Fig. 7. Time-series variation in relative contributions (%) of (a) surface scatter, (b) double-bounce scatter, and (c) volume scatter derived from the Freeman-Durden decomposition.

Fig. 8. Mean JM distance for each crop to the others through the year derived with (a) linear polarization bands (HH, HV, VV), (b) Cloude-Pottier parameters, (c) Freeman-Durden parameters, and (d) all available parameters.

Fig. 9. Summer crop examples for corn, sunflower, and tomato. Note that all the photos were taken in the United States by volunteers, and are freely shared by the Earth Observation and Modeling Facility (EOMF) at the University of Oklahoma (http://eomf.ou.edu/visualization/gmap/).

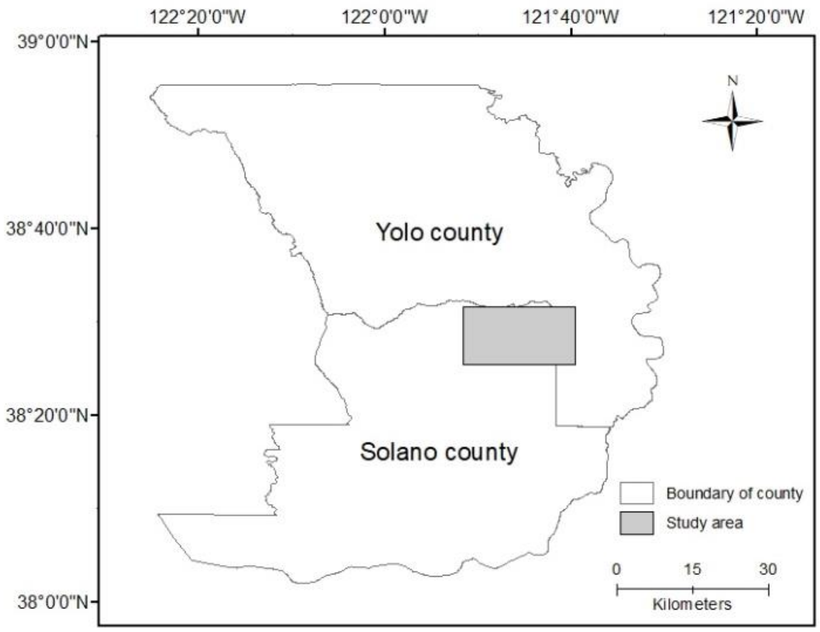

Fig. 1. The study site in the agricultural region of the Sacramento Valley, California.

(a)

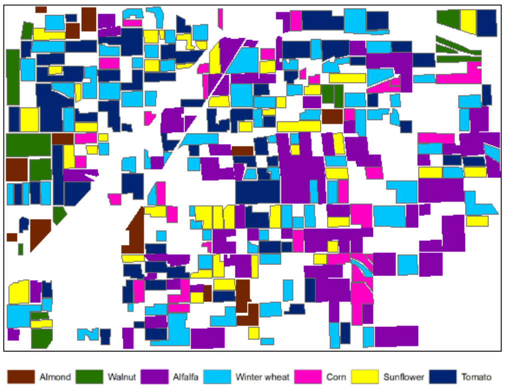

(b)

Fig. 2. (a) The UAVSAR image dated 20 July, 2011 (R-G-B, bands VV, HV, and HH), (b) the outlined crop fields.

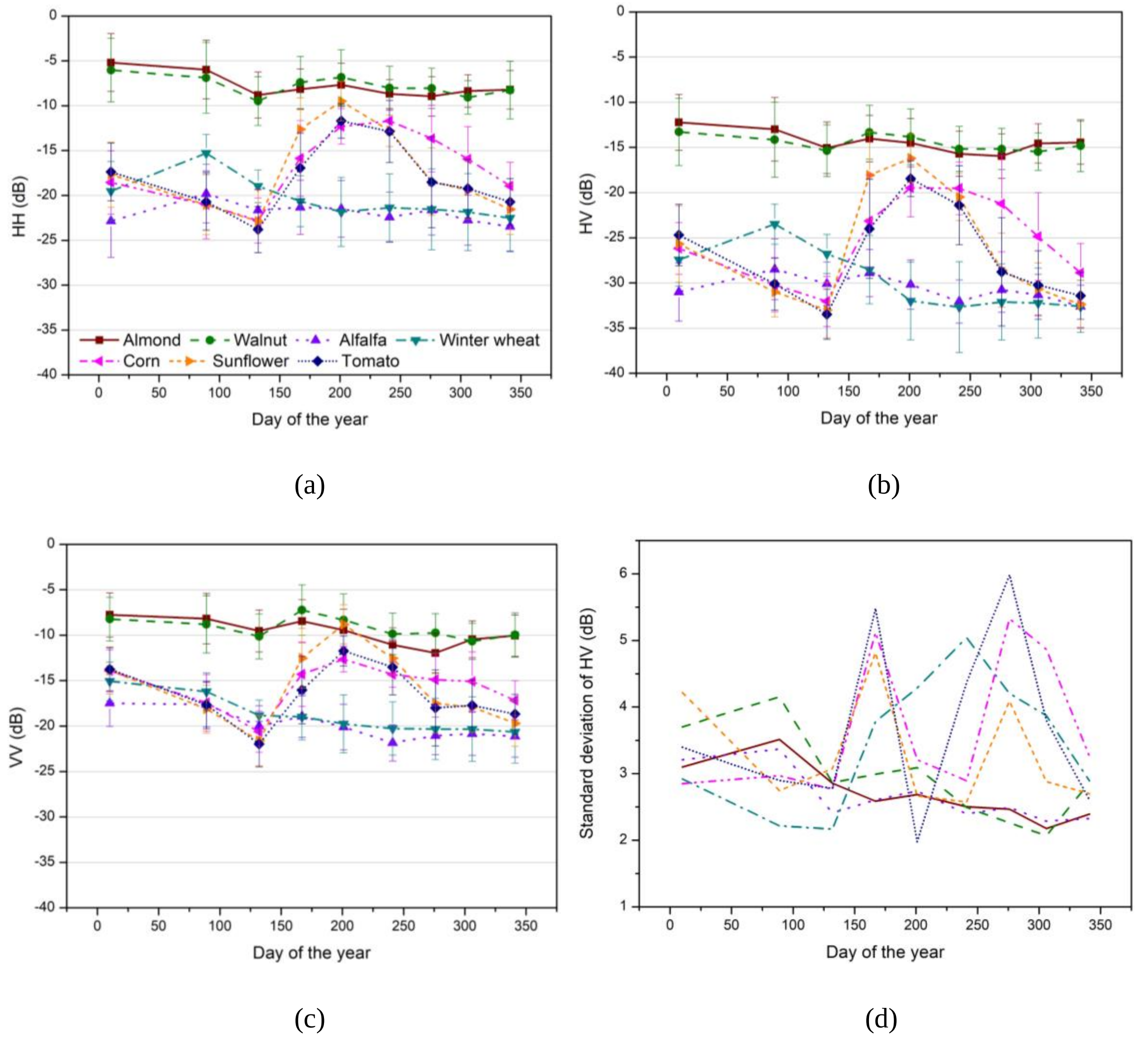

(a) (b)

(c) (d)

Fig. 3. Temporal variation in average backscattering values for crops over linear polarizations (a) HH, (b) HV, (c) VV; Note error bars denote standard deviation. (d) standard deviation profile with HV polarization was depicted separately for analysis.

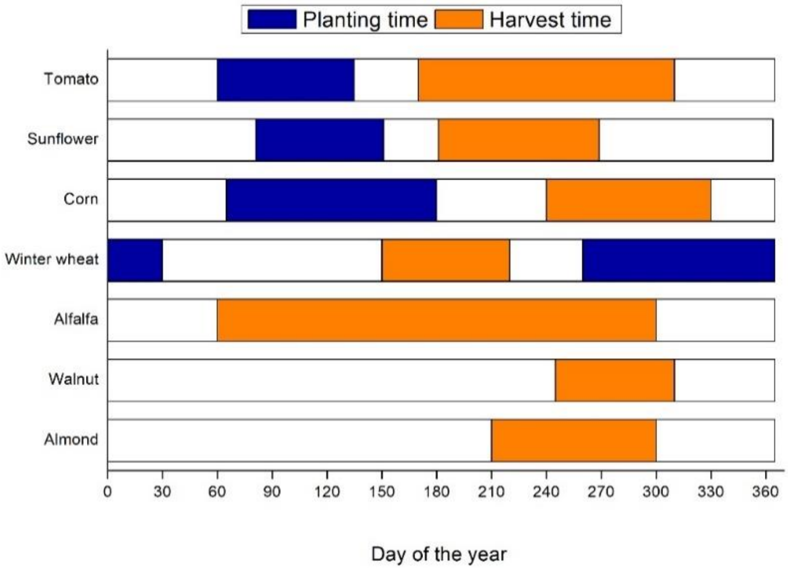

Fig. 4. Crop calendar for the seven major crops in the study area. Note there is no planting time for the perennial almond, walnut, and alfalfa crops.

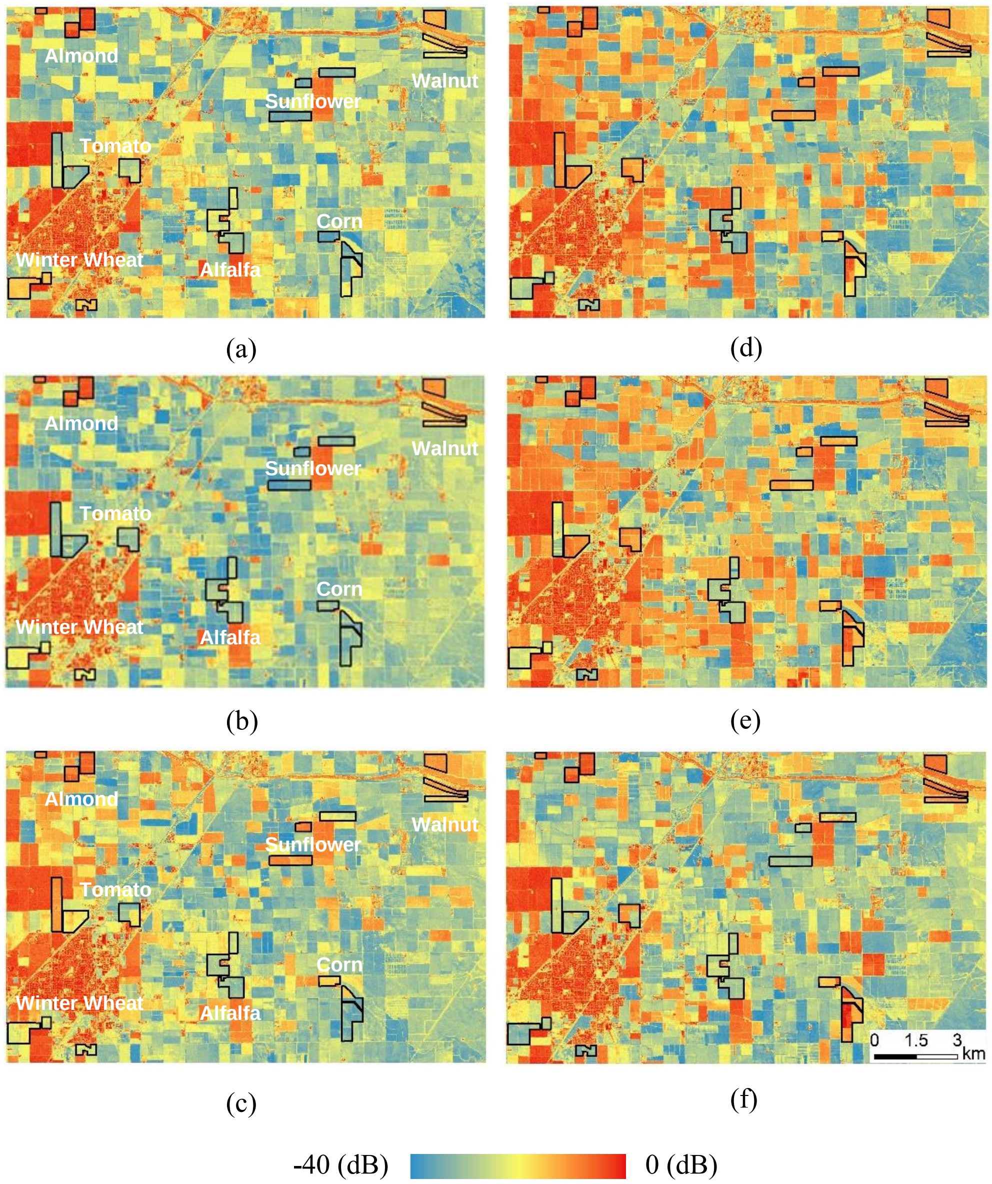

Fig. 5. Radar backscattering values (HV polarization) shown in the UAVSAR images dated (a) 30 March (b) 12 May, (c) 16 June, (d) 20 July, (e) 29 August, and (f) 03 October. Note typical fields for the studied crops were marked by black patches.

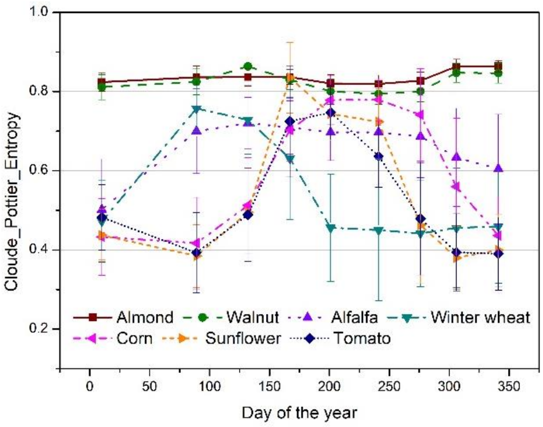

(a)

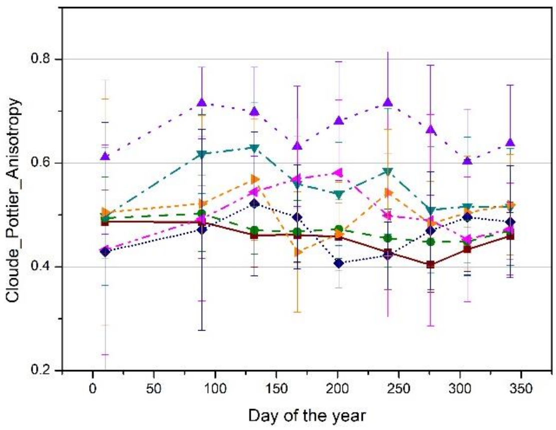

(b)

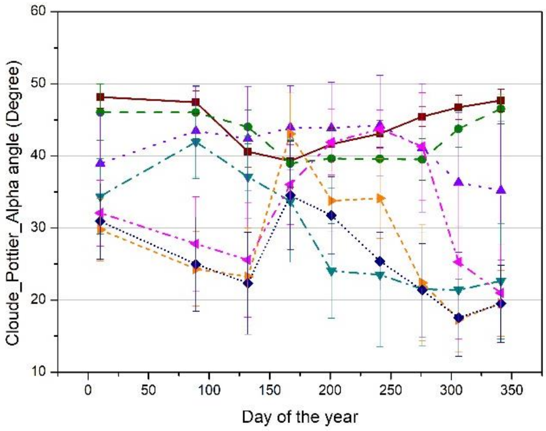

(c)

Fig. 6. Time-series variation in average (a) entropy, (b) anisotropy, and (c) alpha angle derived from the Cloude-Pottier decomposition. Note error bars denote standard deviation.

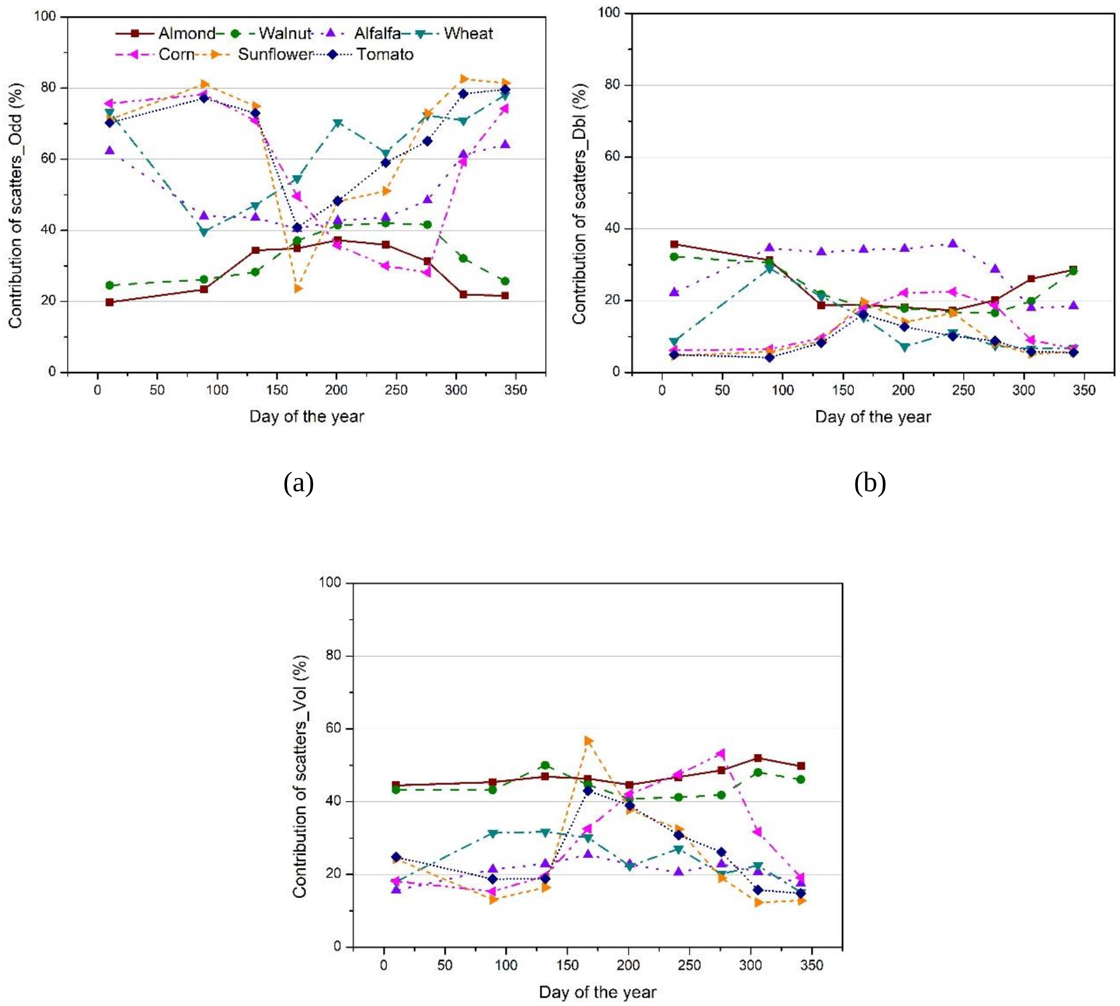

(a) (b)

(c)

Fig. 7. Time-series variation in relative contributions (%) of (a) surface scatter, (b) double-bounce scatter, and (c) volume scatter derived from the Freeman-Durden decomposition.

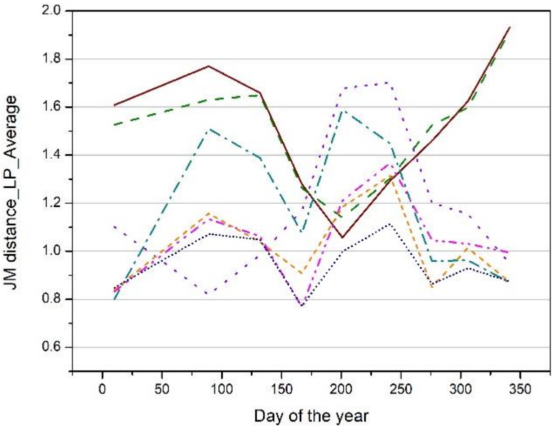

(a)

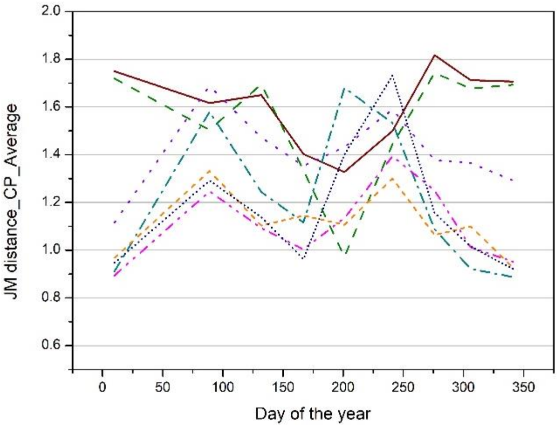

(b)

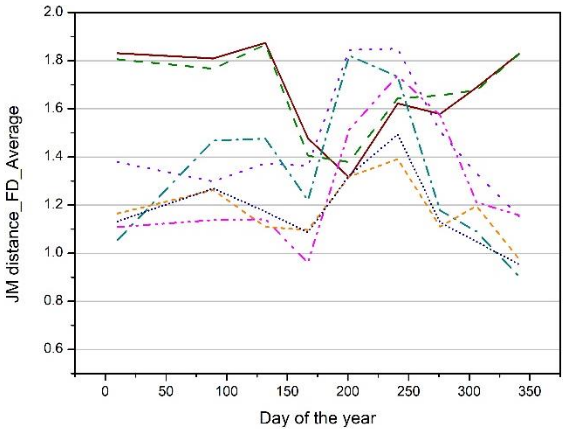

(c)

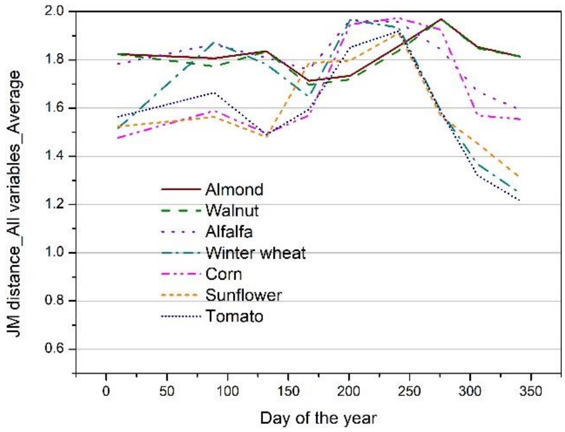

(d)

Fig. 8. Mean JM distance for each crop to the others through the year derived with (a) linear polarization bands (HH, HV, VV), (b) Cloude-Pottier parameters, (c) Freeman-Durden parameters, and (d) all available parameters.

Corn Sunflower Tomato

Fig. 9. Summer crop examples for corn, sunflower, and tomato. Note that all the photos were taken in the United States by volunteers, and are freely shared by the Earth Observation and Modeling Facility (EOMF) at the University of Oklahoma (http://eomf.ou.edu/visualization/gmap/).

Table Captions

Table 1. Detailed description of UAVSAR data acquisitions in 2011 and the corresponding weather conditions; meteorological data were acquired from a station (in the city of Sacramento) located next to the study area (NOAA-NCEI, 2011). All images were in PolSAR (polarimetric SAR) mode and there was no snow.

Table 2. Growing season JM distance values for all crop type pairs calculated with linear polarizations (LP), Cloude–Pottier (CP), Freeman–Durden (FD), and all parameters, respectively.

Table 3. Classification accuracy achieved by the MLP and SVM algorithms with linear polarizations (LP), CP decomposition parameters (CP), FD decomposition parameters (FD), and all features (All). Note that OA denotes overall accuracy, and *k* is the Kappa coefficient.

Table 1

Detailed description of UAVSAR data acquisitions in 2011 and the corresponding weather conditions; meteorological data were acquired from a station (in the city of Sacramento) located next to the study area (NOAA-NCEI, 2011). All images were in PolSAR (polarimetric SAR) mode and there was no snow.

Date	Local time	T_{max} (°C)	T_{min} (°C)	P_{daily} (mm)
10 January	20h59	8.3	-2.8	0
30 March	20h00	26.7	11.7	0
12 May	22h22	26.1	9.4	0
16 June	13h04	31.1	14.4	0
20 July	18h54	35.6	15.0	0
29 August	20h21	34.4	14.4	0
03 October	22h02	20.6	10.0	0.5
02 November	22h45	22.8	5.6	0
07 December	20h20	14.4	-0.6	0

Note that T_{max} and T_{min} are daily maximum and minimum air temperatures, respectively, and P_{daily} signifies daily precipitation.

Table 2

Growing season JM distance values for all crop type pairs calculated with linear polarizations (LP), Cloude–Pottier (CP), Freeman–Durden (FD), and all parameters (LP+CP+FD), respectively.

	JM distance					JM distance			
Class pairs	LP	CP	FD	All	Class pairs	LP	CP	FD	All
Alm--Wal	1.747	1.962	1.974	2	Alf--Whe	1.845	1.967	1.961	2
Alm--Alf	2	2	2	2	Alf--Cor	2	1.986	2	2
Alm--Whe	2	2	2	2	Alf--Sun	2	1.998	2	2
Alm--Cor	2	2	2	2	Alf--Tom	1.998	1.999	2	2
Alm--Sun	2	2	2	2	Whe--Cor	2	1.999	2	2
Alm--Tom	2	2	2	2	Whe--Sun	2	2	2	2
Wal--Alf	2	2	2	2	Whe--Tom	1.999	1.999	2	2
Wal--Whe	2	2	2	2	Cor--Sun	1.959	1.991	1.996	2
Wal--Cor	2	2	2	2	Cor--Tom	1.897	2	1.997	2
Wal--Sun	2	2	2	2	Sun--Tom	1.711	1.891	1.962	2
Wal--Tom	2	2	2	2	-	-	-	-	-

Note that Alm, Wal, Alf, Whe, Cor, Sun, and Tom denote abbreviation of almond, walnut, alfalfa, winter wheat, corn, sunflower, and tomato, respectively. The expression 'Alm--Wal' denotes a class pair between almond and walnut, and so forth.

Table 3

Classification accuracy achieved by the MLP and SVM algorithms with linear polarizations (LP), CP decomposition parameters (CP), FD decomposition parameters (FD), and all features (All). Note that OA denotes overall accuracy, and k is the Kappa coefficient.

Method	Accuracy	Features			
		LP	CP	FD	All
MLP	OA	89.23%	93.01%	93.71%	95.80%
	k	0.8680	0.9146	0.9229	0.9486
SVM	OA	84.48%	92.03%	93.01%	97.48%
	k	0.8085	0.9022	0.9141	0.9691